GA–A25792

INTEGRATED SCENARIO MODELING FOR STEADY STATE OPERATION IN DIII-D AND ITER

by
M. MURAKAMI, J.M. PARK, H.E. St. JOHN,
C.E. KESSEL, and the DIII-D TEAM

MAY 2007

GENERAL ATOMICS

DISCLAIMER

GA–A25792

INTEGRATED SCENARIO MODELING FOR STEADY STATE OPERATION IN DIII-D AND ITER

by
M. MURAKAMI,* J.M. PARK,* H.E. St. JOHN,
C.E. KESSEL,† and the DIII-D TEAM

This is a preprint of a paper to be presented at the 5th IAEA Technical Meeting on Steady State Operations of Magnetic Fusion Devices, May 14-17, 2007 in Daejeon, Republic of Korea and to be published in the Proceedings.

*Oak Ridge National Laboratory, Oak Ridge, Tennessee
†Princeton Plasma Physics Laboratory, Princeton, New Jersey

Work supported by the
U.S. Department of Energy under
DE-FC02-04ER54698, DE-AC05-00OR22725
and DE-AC02-76CH03073

GENERAL ATOMICS PROJECT 30200
MAY 2007

ABSTRACT

Steady-state operation with fusion gain $Q \geq 5$ is a high level goal for ITER. In order to achieve this goal, operation with q_{95} = 5, β_N = 2.8, bootstrap fraction >50% and a well-aligned plasma current would be required. Advanced Tokamak (AT) research on DIII-D focuses on development of the scientific basis for scenarios that meet this objective. Recent progress in this area includes demonstration of 100% noninductive conditions with high normalized fusion performance, $G = \beta_N H_{89} / q_{95}^2 = 0.3$, meeting performance requirement for the ITER steady state $Q = 5$ scenario. Integrated modeling has been a crucial tool in the DIII–D AT research program. The theory-based (GLF23) model with self-consistent sources and sinks in the ONETWO transport code has been used to design experiments and interpret their results on DIII–D. The same tools were used to extrapolate from DIII-D to ITER, predicting an existence proof of the steady state $Q = 5$ scenario with ITER's "Day-1" heating and current drive capabilities (without LHCD). Recent simulations with the same input power and kinetic profiles, but starting from a broad current profile with $q_{\min} \approx 2$ form a strong, but broad, internal transport barrier (ITB) early, making a significant increase in $T_i(0)$ (factor ≈ 2 with $T_i / T_e \approx 1.5$), and Q increased by 50%, and β_N reaching 3.4. Although it still appears transient, the behavior is reminiscent of the DIII-D experiment where β_N = 4 was maintained for 2 s by starting from a broader current profile using a toroidal field ramp. Work continues to examine if the ITB can be sustained by the off-axis ECCD.

1. INTRODUCTION

Steady-state operation with fusion gain, $Q \geq 5$, is a high level goal for ITER [1]. The goal of the Advanced Tokamak (AT) program on DIII-D [2,3] is to optimize the tokamak concept for attractive fusion energy production. The key elements for the AT operation are: steady state, low recirculating power, compactness, and high power density. These requirements can be represented by the achievement of three parameters simultaneously: high noninductive current fraction, $f_{NI} \approx 100\%$; high bootstrap current fraction, f_{BS}; and normalized fusion performance, $G = \beta_N \mathrm{H}_{89} / q_{95}^2 = 0.3$ [3]. AT experiments on DIII-D aim to integrate these key elements that are required for sustained AT operation [4,5]. Recent efforts focus on two scenarios [6]. One reaches fully noninductive conditions ($f_{NI} \approx 100\%$) at $G \approx 0.3$ [7], consistent with the performance of the ITER $Q = 5$ steady-state scenario. The other scenario exhibits very high fusion performance, $G \leq 0.7$ with internal transport barrier (ITB), but is not stationary [8].

Efforts in the first scenario emphasize optimization of fully noninductive operation by operating at $1.5 < q_{\min} < 2.0$ with modest reversed shear ($q_0 - q_{\min} \leq 0.5$) and maintaining the current by bootstrap, neutral beam (NB) and electron cyclotron current drive (ECCD) at $\beta_N \leq 3.5$. Figure 1 shows that a growing number of DIII-D discharges have demonstrated $f_{NI} \approx 100\%$ and exceeded $G \approx 0.3$, indicating that the performance required for the ITER steady-state scenario has been demonstrated. Figures 2 and 3 show characteristics of a typical discharge in which a 100% noninductive condition has been achieved both globally and locally across the plasma [7]. These conditions are achieved at $\beta_N \approx 3.5$: $f_{NI} \approx 100\%$ lasted for up to one half of current relaxation time [9]. Similar plasmas have been obtained $f_{NI} \geq 95\%$ limited only by the 2 s ($\approx \tau_R$) duration of ECCD hardware. The typical current components are: $f_{BS} \approx$ 50–65%, $f_{NB} \approx$ 20–35%, and $f_{EC} \approx$ 5–10%. The performance in these AT experiments meets or exceeds requirements for ITER $Q = 5$ steady-state scenario.

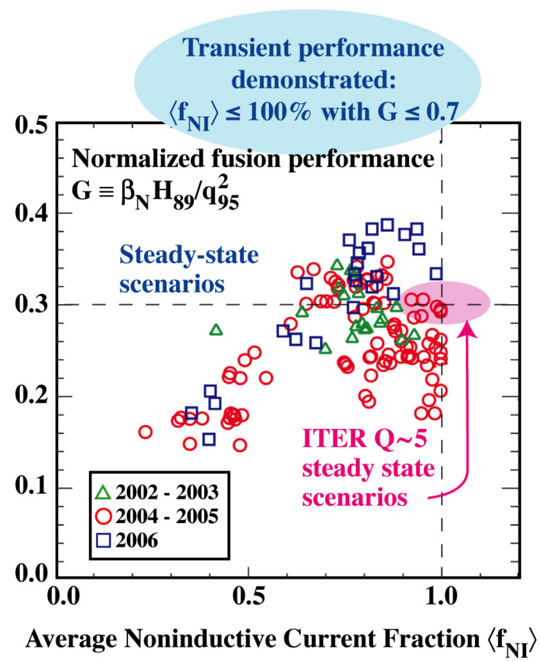

Fig. 1. Normalized fusion performance versus average noninductive current fraction in the DIII-D global database. Growing numbers of shots approach the ITER steady state scenario target. Another scenario has demonstrated high performance close to full noninductive operation, although transient.

The highlight of the efforts for the second scenario is access to $\beta_N \approx 4 (\approx 6 \ell_i)$, well above the no-wall stability limit, sustained for 2 s with internal transport barriers [8]. The current profile is broadened by a combination of ECCD and a toroidal magnetic field ramp that drives some off-axis current [6], which helps improve coupling with the wall and the active control coils. Although this method of driving current does not extrapolate to steady state, these results demonstrate the value of far off-axis current drive, which in future experiments may be provided by other means. We will come back to this later.

The steady state AT existence proof was obtained through strong coupling between integrated modeling and experiment. The theory-based, gyro-Landau fluid (GLF23) model [10,11] with self-consistent sources and sinks within the ONETWO transport code [12] is routinely used both for designing experiments and for interpreting their results in DIII-D [13]. Repeated cycles of modeling and data interpretation help develop the modeling tools that are validated against experiments. The same model is applied to ITER simulations. Benefits of the coupling with experiment are not just validation of the model but also development of optimized approaches to the ITER steady state scenario [7].

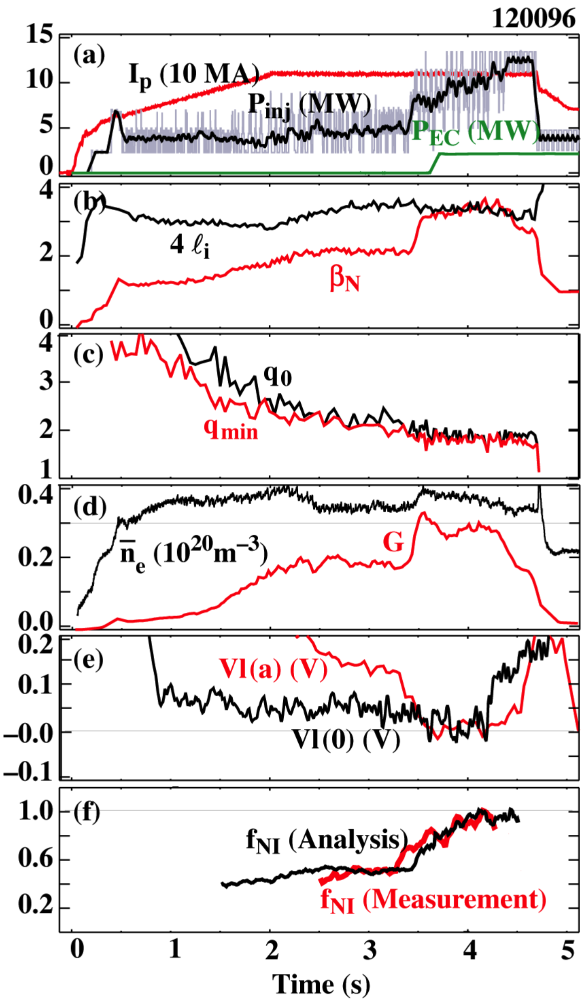

Fig. 2. Evolution of plasma characteristics of a DIII-D discharge with noninductive current fraction $f_{NI} \approx 100\%$ and $G \approx 0.3$ with improved CD alignment: (a) plasma current, NBI and ECCD power; (b) normalized beta and four times internal inductance (approximately no-wall limit); (c) central and minimum safety factor; (d) line-average electron density and normalized fusion performance, $G = \beta_N H_{89} / q_{95}^2$; (e) surface and axial loop voltage; and (f) noninductive current fractions from the internal loop voltage and transport analysis.

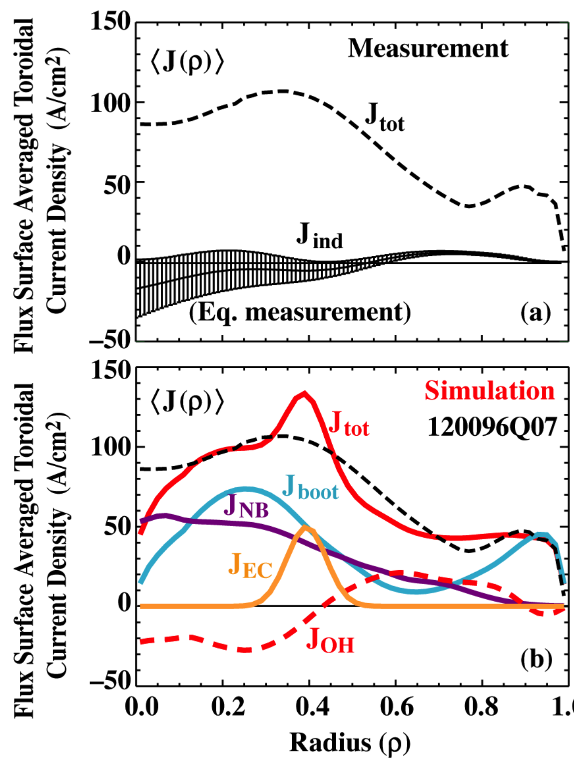

Fig. 3. Current profiles of the $f_{NI} \approx 100\%$ discharge shown in Fig. 2 showing that the inductive (Ohmic) current is globally and locally small: (a) Inductive current derived from the loop voltage analysis based on equilibrium reconstruction; (b) Analysis and simulation of noninductive current using a transport code showing that noninductive current components add up to almost 100%, in agreement with the measurement.

In this paper, we discuss in Section 2 the modeling tools and their validation against experiments that aim at steady state AT operation in DIII-D. Section 3 will discuss simulations of the ITER steady state $Q=5$ scenario using the ITER Day-1 heating and current drive capabilities. The simulations indicate existence of $f_{NI}=100\%$ with $Q=5$. Some uncertainties and future studies are pointed out. Section 4 discusses similar simulations but with internal transport barrier, which improves performance but still falls short of achieving the steady state goal. Section 5 concludes the paper.

2. MODELING TOOLS AND VALIDATION AGAINST EXPERIMENTS

The ONETWO transport code [12] solves the flux surface averaged transport equations for energy (T_e and T_i), particle density, toroidal rotation, current density (or more precisely poloidal magnetic field) and equilibrium evolution using the GLF23 transport model with self-consistent source and sink calculations. The GLF23 model (specifically, the "renormalized" version [11]) uses drift-wave eigenmodes in computing the quasi-linear energy and toroidal momentum fluxes due to ion/electron temperature gradient (ITG/ETG) modes and trapped electron modes (TEM). The model includes $\mathrm{E} \times \mathrm{B}$ shear and alpha-stabilization using the predicted profiles. The electron and ion turbulent diffusivities from GLF23 are added to the neoclassical diffusivities, while the turbulent driven toroidal momentum transport is added to an ad hoc value, twice the neoclassical ion thermal diffusivity, as in Ref. [11]. Although the density equation can be solved with the GLF23 model, most of the simulations discussed here use the density profile from experiments. Solving the highly nonlinear, stiff transport model is facilitated by a novel numerical algorithm: globally convergent Newton method (GCNM) [14], based on modified Newton, thrust region, and steepest descent methods. Taking advantage of the GCNM, a steady state scenario with fully penetrated current profile is obtained by interleaving time-stepping calculation of all the transport equations with a one-step solution of current evolution. The source models used for ITER simulations with ONETWO are the ray tracing codes, TORAY-GA [15] for electron cyclotron (EC) and CURRAY [16] for fast wave (FW), and the Monte-Carlo code NUBEAM [17] for neutral beam heating and current drive. A computational efficiency has been improved by a recent parallelization of ONETWO [18].

The ONETWO/GLF23 model is validated against DIII-D experiments that aim at fully non-inductive operation at high beta. The experimental data in Fig. 4 were chosen to be at the same phase (70±10%) of the ELM cycle in a stationary part of the discharge using the tools developed for pedestal studies [19]. The boundary conditions were taken at $\rho = 0.9$ based on ELM-averaged experimental profiles (with $\beta_{ped} \approx 1\%$). The predicted T_e and T_i profiles reproduce reasonably well the experimental profiles, while the toroidal rotation (Ω_{rot}) profile somewhat overestimates the measured rotation near the axis despite an additional *ad hoc* factor (twice the ion thermal neoclassical value) in the momentum diffusivity [7].

The modeling has been also validated against parametric dependences in a series of steady state AT experiment on DIII-D. As seen in Fig. 5, the ONETWO/GLF23 model also reproduces reasonably well the trend of the noninductive current components in DIII-D density scan data. These exercises help plan optimization experiments as well as simulation optimization.

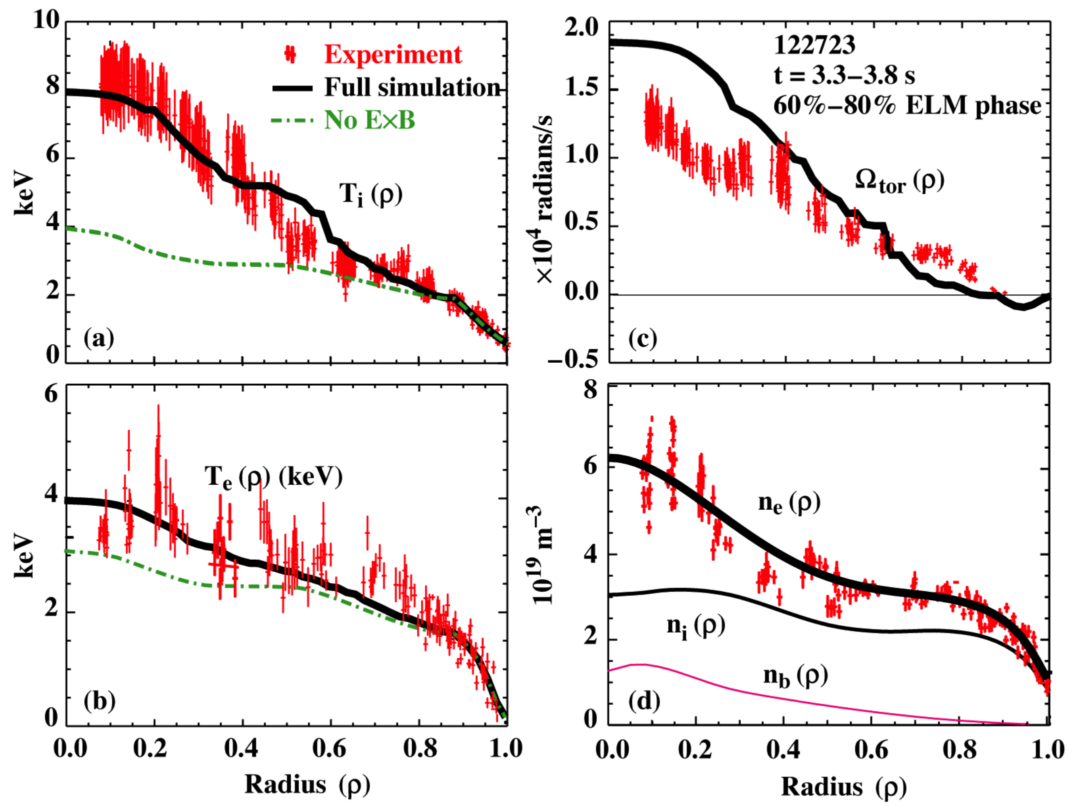

Fig. 4. Theory-based (GLF23) model predictions agree with experimental measurements of profiles of: (a) ion temperature; (b) electron temperature; (c) toroidal angular rotation velocity. The transport simulation uses the prescribed density profile (d) and boundary conditions based on experimental pedestal values at normalized radius of 0.9.

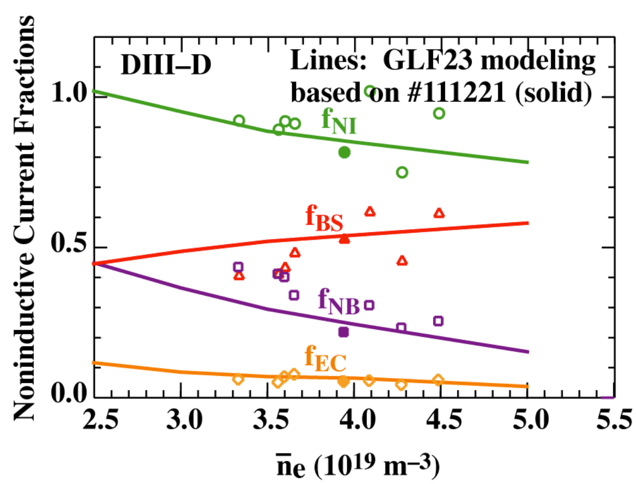

Fig. 5. Predictions of transport simulation on electron density dependence of noninductive current fraction and its components (shown by the solid curves) compared with analysis of experimental data (shown by points): noninductive current (circle), bootstrap current (triangle), neutral beam current drive (square); electron cyclotron current drive (diamond).

3. ITER STEADY STATE SCENARIO MODELING

The modeling tools successfully employed to devise experiments in DIII-D are applied to the steady state $Q \approx 5$ scenario for ITER with Day-1 hardware capabilities. The goal of the steady state operation is a demonstration of fully noninductive current drive with fusion gain $Q > 5$ over the duration of at least 3000 s [1]. In order to achieve this goal, operation with I_p = 9 MA, q_{95} = 5, β_N = 2.8, H_{98} = 1.6 with burn time of 3000 s would be required. In addition, both plasma and bootstrap currents need to be well aligned with f_{BS} to be at least ~50%. The Day-1 heating and current drive capabilities assumed are: negative-ion based NBI (1 MeV, 33 MW, fully steered 0.40 m downwards from the machine elevation at the tangency radius of 5.3 m), FW heating and current drive (20 MW, 56 MHz, second T harmonic) and EC heating and current drive (170 GHz, 20 MW, top launch steered for off-axis CD). This list does not include lower hybrid current drive (LHCD).

Each ITER scenario modeling effort needs some exploratory parameter scans to set important simulation parameters, such as boundary conditions or optimal density values. Previously, we showed an "existence proof" of full noninductive operation at $Q \approx 5$ at high density (Greenwald number $N_{GW} = 1.25$) using the GLF23 model with the ITER Day-1 hardware capabilities [20,21]. A similar scan indicates that pedestal temperature at $\rho = 0.9$, $T_{ped}(\rho = 0.9) \approx$ 8 keV is needed. We also evaluate how the noninductive operation would change when the plasma density is varied as in DIII-D. Fractions of the noninductive current components and fusion gain, G, are plotted as a function of Greenwald number (Fig. 6). The trend of the noninductive current fraction is reminiscent of those for the DIII-D density scan (Fig. 5). Increased noninductive fraction above 100% is attained at Greenwald number (N_{GW}) below 1 with only a modest reduction of fusion gain, Q.

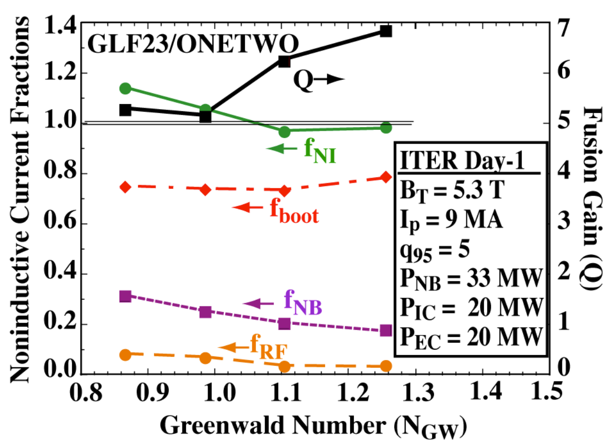

Fig. 6. Density dependence of the noninductive current fraction and its component, and fusion gain predicted by the GLF23 modeling using the ITER Day-1 hardware capabilities.

Taking the optimal density case in the exploratory density scan, we focus on the $N_{GW} \approx 1$ case, with $f_{NI} = 100\%$ and $Q = 5$. The details of the simulation specifications are similar to those described in Ref. [22]. The electron density profile is specified as $n(\rho = 0.8) = n(0) = 0.85 \times 10^{20}$ m^{-3}, and to $0.35 \times n(0)$ at the separatrix. This gives a very broad profile with a peak-to-volume average of about 1.2. The DT fuel ion ratio is assumed to be 50-50. The impurities are Be and Ar, with assumed fractions of 2% and 0.12%, respectively, with the same impurity density profile shape as the electron density. The fuel ion density profiles are determined from quasi-neutrality. These give the effective charge, Z_{eff}, of 1.73 on axis and 1.60 at the edge. The T_e and T_i at the boundary are set to $T(\rho = 0.9) = 8$ keV, and are forced to be 200 eV at the separatrix. The ratio of the effective particle to energy confinement time ($\tau_p^* / \tau_{\mathrm{E}}$) is ≈ 9. The ONETWO transport code solves T_e, T_i, Ω, and J equations using the GLF23 core transport model with all boundary conditions at $\rho = 0.8$.

The long current relaxation time and small time steps required for the stiff transport model require a two-step simulation process: step #1: Time stepping for >100-s (~1 τ_R for ITER) for T_e, T_i, Ω, and J evolution, and step #2: Time stepping for >1000 s time of J-evolution alone by solving Faraday's law using the previously determined T_e, T_i, and Ω as initial conditions. This Step #2 can be (and is) replaced with "one-step steady-state" calculation, thanks to the above-mentioned GCNM algorithm. If necessary steps #1 and #2 can be iterated. Shown in Fig. 7 are the time evolutions of T_{e0}, T_{i0}, q_0 and $q_{\min}$ and the evolutions of noninductive current fractions and fusion gain for step #1 (for 250 s) and #2 for J-evolution toward steady state. Over the initial 250 s ($\approx 2\ \tau_R$), relatively small changes happen in these parameters, except an initial excursion of q_0. During the J relaxation phase, the q profile recovers a modest central magnetic shear toward the steady state. Figure 8 shows profiles of T_e, T_i, densities Ω, noninductive current components, and safety factor at 250 s and at steady state. This simulation (Case A) projects to an ITER steady state scenario that achieves $f_{NI} = 109\%$ and $Q = 5.5$ with $f_{BS} = 80\%$ and $T_e(0) \approx T_i(0) \approx 22$ keV at $I_p = 9$ MA and $B_T = 5.3$ T, as listed in Table 1. The excess 9% in noninductive fraction can provide a margin for control of the operation point.

Integrated modeling suggests hardware for desirable performance improvements. Both off-axis and axial current drive are needed to control high bootstrap fraction AT plasmas. Large negative magnetic shear reduces the beta limit due to peaked pressure profile, while elevated q would help to increase the bootstrap fraction. Figure 9(a) shows the electron and ion heating power density profiles, while Fig. 9(b) shows the current drive profiles for EC, FW and NB for the steady state portion of Case A. Note that for Case A, only 50% of full FWCD is used since full FWCD capability would have pushed q_0 down below $q = 1$.

FWCD can furnish a fine control of the central magnetic shear ($\Delta q = q_0 - q_{\min}$) to compensate the time-varying axial ohmic current. Co current drive is needed to minimize the initial transient excursion of Δq as J_{OH} penetrates at an early stage. Toward steady state, depending on over-drive or under-drive by the other CD sources, co- or counter-current drive is needed for an optimal q profile. It is possible to control the amount of CD by changing the duration of the co- and counter-phasing of antenna spectra ("dwell control"). A feedback control algorithm similar to that in the DIII-D Plasma Control System (PCS) [23] has been implemented for this purpose [24]. With this feedback control, it is possible in the simulation to maintain $q_{\min} > 1.5$ and $\Delta q = q_0 - q_{\min} \approx 0.5$ for the entire discharge duration.

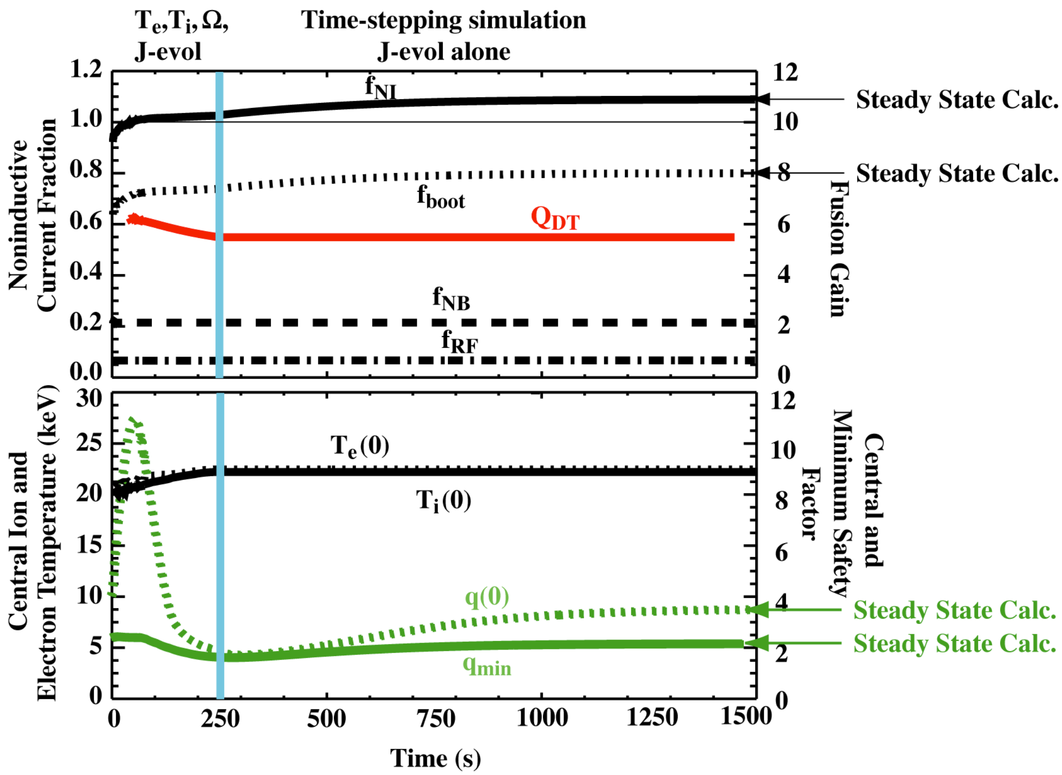

Fig. 7. Two step simulation process used for ITE steady-state performance prediction: Time stepping calculations of T_e, T_i and rotation, plasma current using the GLF23 model for initial 250-s period; and then calculations of current evolution alone while keeping fixed the profiles of the final solutions at the first step.

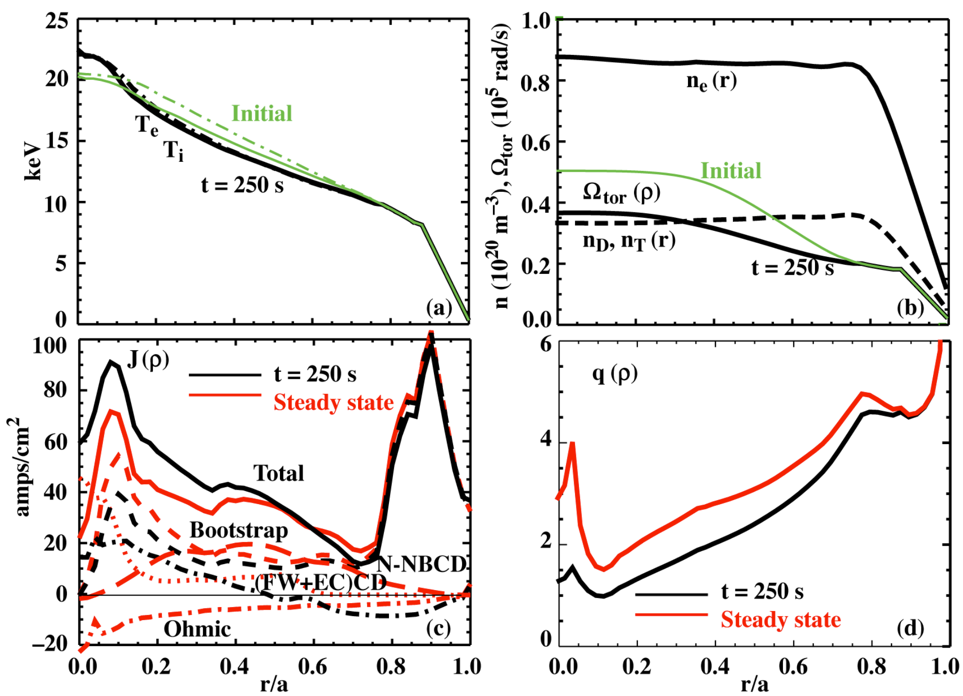

Fig. 8. Predictive modeling of ITER steady state scenario using the GLF23 transport model: (a) predicted electron and ion temperature profiles, (b) assumed electron, deuterium and tritium density profiles, and predicted toroidal angular rotation velocity, (c) current components, and (d) safety factor profiles.

Table 1
Parameters Used and Obtained from Simulations with ONETWO/GLF23 Model for Two Cases: Case A [Without Internal Transport Barrier (ITB)], and Case B (with ITB)

	Case A	Case B		Case A	Case B
I_p (MA)	9.0	9.0	f_{BS}	0.8	0.58
B_T (T)	5.3	5.3	f_{NB}	0.21	0.24
R (m)	6.2	6.2	f_{EC}	0.04	0.04
a (m)	1.86	1.8	f_{FW}	0.03	0.03
Elongation	1.98	1.75	f_{NI}	1.08	0.89
Volume	795.0	693.0	$n_e(0)$ (10^{20} m^{-3})	0.875	0.801
P_{NB} (MW)	33.0	33.0	$\bar{n}_e$ (10^{20} m^{-3})	0.741	0.676
P_{EC} (MW)	20.0	20.0	$T_e(0)$ (keV)	22.4	23.6
P_{FW} (MW)	20	20.0	$T_i(0)$ (keV)	22.1	32.0
q_{95}	5.54	5.5	$\langle Z_{eff} \rangle$	1.65	1.7
q_0	3.46	7.4	τ_E	2.25	2.61
q_{min}	2.09	1.96	H_{89P}	2.89	3.18
β_N	2.9	3.41	H_{98y2}	1.64	1.65
β_T (%)	2.64	3.1	Q_{fusion}	5.45	7.15

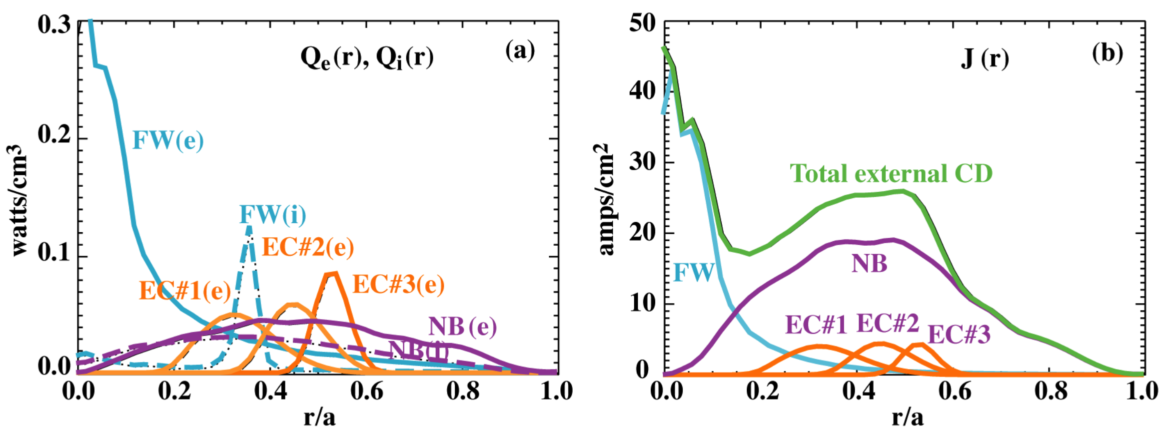

Fig. 9. Profiles of heating and current drive self-consistently calculated for the ITER Day-1 hardware, negative-ion based neutral beam (NB), electron cyclotron (EC) and fast wave (FW) systems: (a) electron and ion heating power deposition profiles, (b) current drive profiles.

Larger off-axis CD in the outer part of the plasma (such as higher-power ECCD or the more efficient LHCD) is highly desirable for a steady state scenario. Due to the limited off-axis ECCD, the above scenario modeling requires a high pedestal temperature, which yields a high bootstrap current at the edge, making control of plasma boundary difficult. A related issue is the density profile. The density profile used in the present modeling originates from the one used in an earlier ITER simulation study [24] as an ion density profile similar to that of a DIII-D AT discharge. Also the density selected is relatively low, to improve the CD effectiveness. Compatibility between edge and divertor under these conditions remains to be addressed. The large pedestal width assumed in the simulation gives a larger stability margin for peeling-ballooning modes [25]. Although the temperature at the peak of the bootstrap current is high ($T_{ped} = 7$ keV), the broader density pedestal width makes the pedestal β (0.9%) only slightly above the DIII-D highest β_{ped} (1.35%) for AT plasmas. Nevertheless, these arguments underscore the importance of understanding the edge pedestal in AT plasmas.

MHD stability, in particular to the resistive wall mode (RWM), is yet to be addressed. The target β_N of 2.9 is above the beta limit for the $n = 1$ mode without conducting wall ($\beta_N^{no-wall} \approx 2.4 - 2.5$) [26,27]. Although the predicted central plasma rotation frequency is about 2.5% of the Alfvén frequency, uncertainties in the simulation (e.g., empirical addition of the neoclassical ion thermal diffusivity in the momentum diffusivity) make it unclear whether it is sufficient to provide RWM stabilization without an active feedback system. DIII-D experiments with the external and internal control coils and the capability to produce nonrotating high beta plasmas using co- and counter-NBI are under way to study the effectiveness of feedback stabilization under more ITER-relevant conditions.

4. SCENARIO MODELING WITH INTERNAL TRANSPORT BARRIER

An alternative to off-axis CD is to find a way to maintain high temperature in the core through an internal transport barrier (ITB). Negative central shear and sheared E×B flow can lead to improved core confinement. Recent simulations have found an ITB in ITER steady-state simulations using a free-boundary ITER equilibrium with a smaller plasma volume (693 m^3 rather than the standard 795 m^3). Although we now have found ITB cases with a standard volume, they tend to be more transient than those with a smaller volume. With small-volume ITER equilibrium, a simulation with the same input power and kinetic profiles, but starting from a broad current profile [as indicated by $\rho\,(q_{\min}) \approx 0.6$ and $q_{\min} \approx 2$] form a strong but broad ITB early, making $T_i\,(0)$ increase by factor ≈ 1.8 (with $T_i/T_e \approx 1.3$), Q increase by 50%, and β_N reaching 3.3, as shown in Fig. 10. ITB formation in an ITER steady-state scenario has been observed in other transport simulations using LHCD [28]. The ion temperature ITB originally grows at the location where the magnetic shear is at minimum, i.e., $\rho\,(q_{\min}) \approx 0.6$, and then it propagates inward, making the ITB region wider. To date, however, we have not succeeded in finding an ITB period for longer than 600 s, and the non-inductive fraction in the smaller plasma has been < 85% due to limited off-axis CD power. Although it still appears transient, the behavior is very much reminiscent of the DIII-D experiment where $\beta_N = 4\,(\approx 6\,\ell_i)$ was maintained for 2 s [8]. Work continues to examine if the ITB can be sustained by the off-axis ECCD. Table I also tabulates the simulation results with ITB ("Case B").

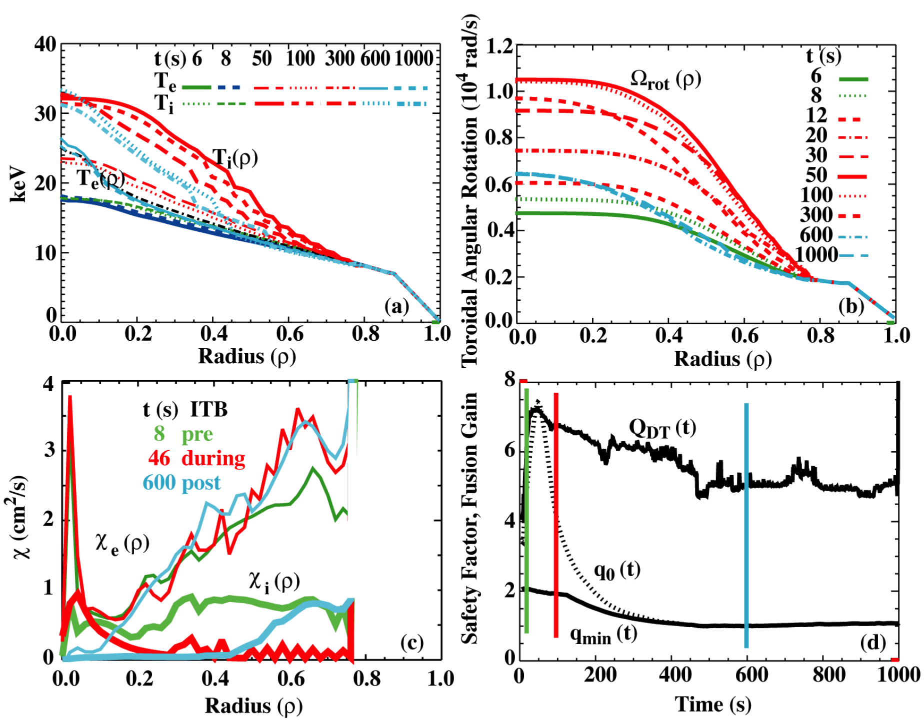

Fig. 10. Evolution of internal transport barrier (ITB) formed in transport simulation and its effects on performance in pre-ITB (green), during ITB (red) and post-ITB (blue) phases: (a) ion and electron temperature profiles, (b) toroidal angular rotation velocity profiles, (c) electron and ion thermal diffusivity, and (d) time histories of fusion gain and minimum safety factor.

5. CONCLUSIONS

Integrated modeling contributed strongly to successful demonstration of 100% noninductive, high β DIII-D experiments. Theory-based GLF23 modeling with self-consistent sources and sinks had been continuously used to plan experiments and interpret their results and continuously improved. The same tools were used to extrapolate from DIII-D to ITER, resulting in an existence proof for the ITER steady-state $Q = 5$ scenario with ITER Day-1 capabilities. Recent simulations produced ITB by starting a broad current profile with smaller plasma volume. However, maintaining ITB for a longer period will likely require stronger off-axis CD. Through coupling between experiment and modeling, good progress has been made in developing a scientific basis to establish steady-state scenarios for ITER and beyond.

ACKNOWLEDGMENTS

This work supported by the U.S. Department of Energy under DE-FC02-04ER54698, DE-AC05-00OR22725 and DE-AC02-76CH03073. We would like to thank the DIII-D experimental staff, in particular, the Advanced Scenario Development Thrust Group, for experimental development efforts for the steady state AT scenarios. The present simulation was, in part, carried out as work for the International Tokamak Physics Activities (ITPA) Steady State Operation (SSO) Working Group, and we would like to acknowledge useful discussions with and encouragement from Dr. C. Gormezano and Dr. A.C.C. Sips.

REFERENCES

[1] Shimomura Y *et al* 2001 *Plasma Phys. Control. Fusion* **43** A385

[2] Taylor T S 1997 *Plasma Phys. Control. Fusion* **39** B47

[3] Luce T C 2005 *Fusion Sci. Technol.* **48** 294004

[4] Murakami M *et al* 2003 *Phys. Rev. Lett.* **90** 255001

[5] Wade M R *et al* 2003 *Nucl. Fusion* **43** 634

[6] Greenfield C M *et al* 2006 *Proc. 21st IAEA Fusion Energy Conf. (Chengdu)* http://www-pub.iaea.org/MTCD/Meetings/FEC2006/ex_1-2

[7] Murakami M *et al* 2006 *Phys. Plasmas* **13** 056106

[8] Garofalo A M *et al* 2006 *Phys. Plasmas* **13** 056110

[9] Mikkelsen D R 1989 *Phys. Fluid B* **1** 333

[10] Waltz R E, Staebler G M, Dorland W, Hammett G W, Kotschenreuther M and Konings J A 1997 *Phys. Plasmas* **4** 2482

[11] Kinsey J E, Staebler G M, Waltz R E 2005 *Phys. Plasmas* **12** 052503

[12] St John H E, Taylor T S, Lin-Liu Y R and Turnbull A D 1995 *Proc. 15th Int. Conf. on Plasma Physics and Control. Nucl. Fusion Research (Seville)* vol 3 (Vienna: IAEA) p 603

[13] Murakami M *et al* 2003 *Phys. Plasmas* **10** 1691

[14] St John H E, Lao L L, Murakami M, Park J M 2006 *Bull. Am. Phys. Soc.* **51** 170

[15] Lin-Liu Y R, Chan V S and Prater R 2003 *Phys. Plasmas* **10** 4064

[16] Mau T K, Chiu S C and Harvey R W 1982 *Proc. EPS Topical Conf. on RF Heating and Current Drive of Fusion Devices (Brussels)* vol 16E (ECA) (Petit-Lancy: European Physical Society) p 181

[17] Pankin A *et al* 2004 *Comput. Phys. Commun.* **159** 157

[18] Park J M *et al* 2006 *Bull. Am. Phys. Soc.* **51** 62

[19] Osborne T H, Burrell K H, Groebner R J, Lao L L, Leonard A W, Maingi R, Miller R L, Porter G D, Staebler G M and Turnbull A D 1999 *J. Nucl. Mater.* **266-269** 131

[20] Murakami M *et al* 2005 Nucl. Fusion **45** 1419

[21] Houlberg W A *et al* 2005 *Nucl. Fusion* **45** 1309

[22] Kessel C E *et al* 2006 Simulation of hybrid and steady state advanced operating modes in ITER *submitted to Nucl. Fusion*

[23] Scoville J T, Humphreys D A, Ferron J R and Gohil P 2006 Simultaneous feedback control of plasma rotation and stored energy on the DIII-D tokamak *Proc. 24th Symp. on Fusion Technology (Warsaw) to be published in Fusion Engin. Design*

[24] Park J M 2007 private communication

[25] Lao L L *et al* 2003 *Nucl. Fusion* **43** 1023

[26] Snyder P B *et al* 2004 *Nucl. Fusion* **44** 320

[27] Liu Y, Bondeson A, Gribov Y and Polevoi A 2004 *Nucl. Fusion* **44** 232

[28] Basiuk V *et al* 2004 *Nucl. Fusion* **43** 320